Biocybernetics and Biomedical Engineering 44 (2024) 358–368

Contents lists available at ScienceDirect

Biocybernetics and Biomedical Engineering

journal homepage: www.elsevier.com/locate/bbe

Research Paper

Modelling the dynamics of microbubble undergoing stable and inertial cavitation: Delineating the effects of ultrasound and microbubble parameters on sonothrombolysis

Zhi Qi Tan [a], Ean Hin Ooi [a,*], Yeong Shiong Chiew [a], Ji Jinn Foo [a], Yin Kwee Ng [b], Ean Tat Ooi [c]

[a] Department of Mechanical Engineering, School of Engineering, Monash University Malaysia, Jalan Lagoon Selatan, 47500 Bandar Sunway, Selangor, Malaysia
[b] School of Mechanical and Aerospace Engineering, College of Engineering, Nanyang Technological University, 50 Nanyang Avenue 639798, Singapore
[c] School of Engineering and Information Technology, Faculty of Science and Technology, Federation University, VIC 3350, Australia

ARTICLE INFO

Keywords:
Acoustic waves
Cavitation
Jet velocity
Thrombolysis
Shear stress

ABSTRACT

Sonothrombolysis induces clot breakdown using ultrasound waves to excite microbubbles. Despite the great potential, selecting optimal ultrasound (frequency and pressure) and microbubble (radius) parameters remains a challenge. To address this, a computational model was developed to investigate the bubble behaviour during sonothrombolysis. The blood and clot were assumed to be non-Newtonian and porous, respectively. The effects of ultrasound and microbubble parameters on flow-induced shear stress on the clot surface during stable and inertial cavitation were investigated. It was found that microbubble translation towards the clot and the shear stress on the clot surface during stable cavitation were significant when the bubble was about to undergo inertial cavitation. While insonation of large microbubble (radius of 1.65 μm) at low frequency (0.50 MHz) produced the highest shear stress during stable cavitation, selection of these parameters is not as intuitive for inertial cavitation due to the strong competing effect between jet velocity and translational distance. An increase in jet velocity is always accompanied by a decrease in the translational distance and vice versa. Therefore, a right balance between the jet velocity and the translational distance is critical to maximise the shear stress on the clot surface. A jet velocity of 303 m/s and a distance travelled of 5.12 μm at an initial bubble-clot separation of 10 μm produced the greatest clot surface shear stress. This is achievable by insonating a 0.55 μm microbubble using 0.50 MHz and 600 kPa ultrasound.

1. Introduction

Health complications caused by blood clots are among the global leading causes of mortality and morbidity. They include ischemic stroke, myocardial infarction, deep vein thrombosis and pulmonary embolism [1]. The most common treatment for blood clot is thrombolytic drugs, such as recombinant tissue plasminogen activator (rt-PA). Nevertheless, this technique is effective only if the drugs can penetrate the clot to induce clot lysis. Hence, a high concentration of rt-PA is often prescribed to increase the chances of clot penetration. Unfortunately, doing so also increases the risk of haemorrhage, with the potential of causing death in patients [2]. As such, there is a demand for better thrombolysis strategies that can improve the thrombolytic effect of drugs. One of the more recent development in this field is sonothrombolysis.

Sonothrombolysis uses ultrasound waves to enhance thrombolytic treatment outcomes [2]. Recent technological advancement has seen the use of various types of ultrasonic systems for sonothrombolysis, which includes high intensity focused ultrasound [3], diagnostic ultrasound systems [4,5], or a forward-viewing intravascular ultrasound transducer [6,7]. The increased efficacy of thrombolytic drugs during sonothrombolysis helps to reduce the dosage of drugs, thus minimising its side effects [6]. During sonothrombolysis, ultrasound oscillations in blood causes the formation of tiny bubbles or acoustic cavitation [8]. Acoustic cavitation can be stable and/or inertial, with both contributing to enhancing thrombolytic outcome, albeit differently. During stable cavitation, the sustained oscillation of the bubble induces hydrodynamic forces that stretches the pores on the clot surface to promote greater drug entry. This is shown in Fig. 1a. Conversely, inertial cavitation is characterised by the violent collapse of the bubble, which often

* Corresponding author.
E-mail address: ooi.ean.hin@monash.edu (E.H. Ooi).

https://doi.org/10.1016/j.bbe.2024.04.003
Received 19 December 2023; Received in revised form 16 March 2024; Accepted 23 April 2024
Available online 4 May 2024

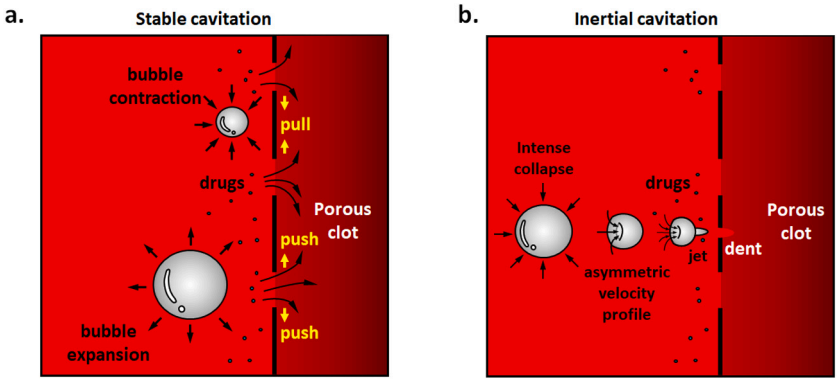

Fig. 1. Schematic of a microbubble undergoing: (a) stable cavitation and (b) inertial cavitation, and their impact on the clot surface.

leads to the development of a high-speed jet [9]. If the collapse occurs next to the clot, the jet will impinge on the clot surface and cause significant clot erosion. This not only breaks down the clot, but also creates dents that increase the surface area for the binding of drugs. This elevates the local drug concentration that helps to break down the clot more effectively [10]. This is shown in Fig. 1b.

To enhance the effect of acoustic cavitation during sonothrombolysis, microbubbles are often introduced intravenously next to the clot [2]. Using an in vitro model, Datta et al. [11] observed an increased rt-PA entry into the clot when microbubbles are used in conjunction with ultrasound at a frequency and pressure amplitude of 120 kHz and 0.32 MPa, respectively. Similarly, Kim et al. [12] reported significant improvement in clot lysis when increasing the microbubble concentration and pressure amplitude at a frequency of 620 kHz. Borrelli et al. [13] discovered that larger microbubbles (3 μm diameter) produced better thrombolytic effects when insonated with low pressure amplitude at a frequency of 1 MHz. Recently, Zhang et al. [14] employed microbubble with average diameter of 1.1 μm to demonstrate the efficacy of a high-speed endovascular sonothrombolysis using vortex ultrasound. Goel et al. [15] discovered that sonothrombolysis using 700 kHz at 0.9 MPa could fragment the clot into tiny debris, thus minimising the risk of embolisation downstream. Although the positive impact of microbubbles were demonstrated, these studies were achieved using different combination of ultrasound frequency and pressure amplitude. Moreover, commercial microbubbles used during sonothrombolysis come in different sizes and concentrations. Hence, this raises the question on what is the optimum combination of ultrasound (frequency and pressure) and microbubble (size and concentration) parameters that produces the best thrombolytic outcome during sonothrombolysis. Unfortunately, this is very difficult to ascertain experimentally due to the large variations in the values of parameters being used [16]. This problem is exacerbated by the difficulty in accurately and reliably performing the experiments in vivo and during inertial cavitation to observe and quantify the bubble dynamics [17].

Computational modelling is an alternative methodology to systematically investigate the bubble dynamics phenomena during sonothrombolysis. This is because computational models provide convenient access to all the parameters of interest for a more consistent comparison of results. Furthermore, parameters that are difficult to measure experimentally, such as the jet velocity and the shear stress acting on the clot surface during jet impingement, can be easily estimated from the numerical solutions [18]. These advantages have led to various researchers employing computational modelling to investigate the bubble dynamics phenomena in blood vessels. For example, Wang et al. [19] employed the boundary element method (BEM) to investigate the nonlinear behaviour of a bubble oscillating in an elastic vessel. Hosseinkhah et al. [20] and Khodabakhshi et al. [21] developed finite element models of the blood–brain barrier to investigate the shear stress acting on the vessel wall due to a pulsating microbubble. More recently, Xie et al. [17] investigated the effects of ultrasound parameters, microbubble size and bubble to wall distance on the risk of vascular injury during acoustic cavitation. These studies highlight the advantages of computational modelling in the study of microbubble dynamics, and their applications in vessel-related complications suggest that there is great potential for it to be extended to sonothrombolysis.

Motivated by this, the present study sets out to develop a computational model that simulates the bubble dynamics phenomena during sonothrombolysis. The model was formulated based on the recent modelling work of bubble dynamics [22–24], which will be used to optimise acoustic cavitation during sonothrombolysis. The present study aims to investigate the effects of ultrasound and microbubble parameters on the characteristics of stable and inertial cavitation. All simulations will be carried out using the commercial software COMSOL Multiphysics. To the authors' knowledge, the present study represents the first attempt at elucidating the dynamics of stable and inertial cavitation during sonothrombolysis with different ultrasound and microbubble parameters. Specifically, this study provides an understanding on the modelling of bubble dynamics next to a porous clot, which has never been explored in the literature. Moreover, the numerical results shed light on the magnitude of flow induced shear stress due to stable and inertial cavitation on the clot surface, which is critical for the selection of the optimum ultrasound and microbubble parameters during sonothrombolysis. As such, the findings from this study may facilitate the optimisation of the treatment and bring sonothrombolysis closer towards clinical implementation.

2. Materials and methods

2.1. Model geometry

Consider a microbubble of radius R_0 located next to a clot in a blood-filled vessel, see Fig. 2a. Since the microbubble is several orders of magnitude smaller than the clot, this allows the computational domain to be truncated to a small region consisting only of the microbubble, the surrounding blood and the clot. To further limit the requirement of computational resources, the model was reduced from 3D to 2D axisymmetry. This is illustrated in Fig. 2a, where $d_{clot} = 10$ μm is the initial distance from the microbubble centre to the clot surface, and L defines the dimension of the truncated model. The value of L was decided based on a preliminary domain convergence study (results not shown) of the temporal response of bubble radius during insonation, where the results indicated that a domain that is at least seven times the maximum expansion radius of the microbubble oscillating in an unbounded domain, *i.e.*, without the clot, was sufficient to minimise undesired boundary effects. Note that the maximum expansion radius of a microbubble oscillating in an unbounded domain is different from that when oscillating next to a clot, and the former is used solely to estimate the dimension of the truncated model.

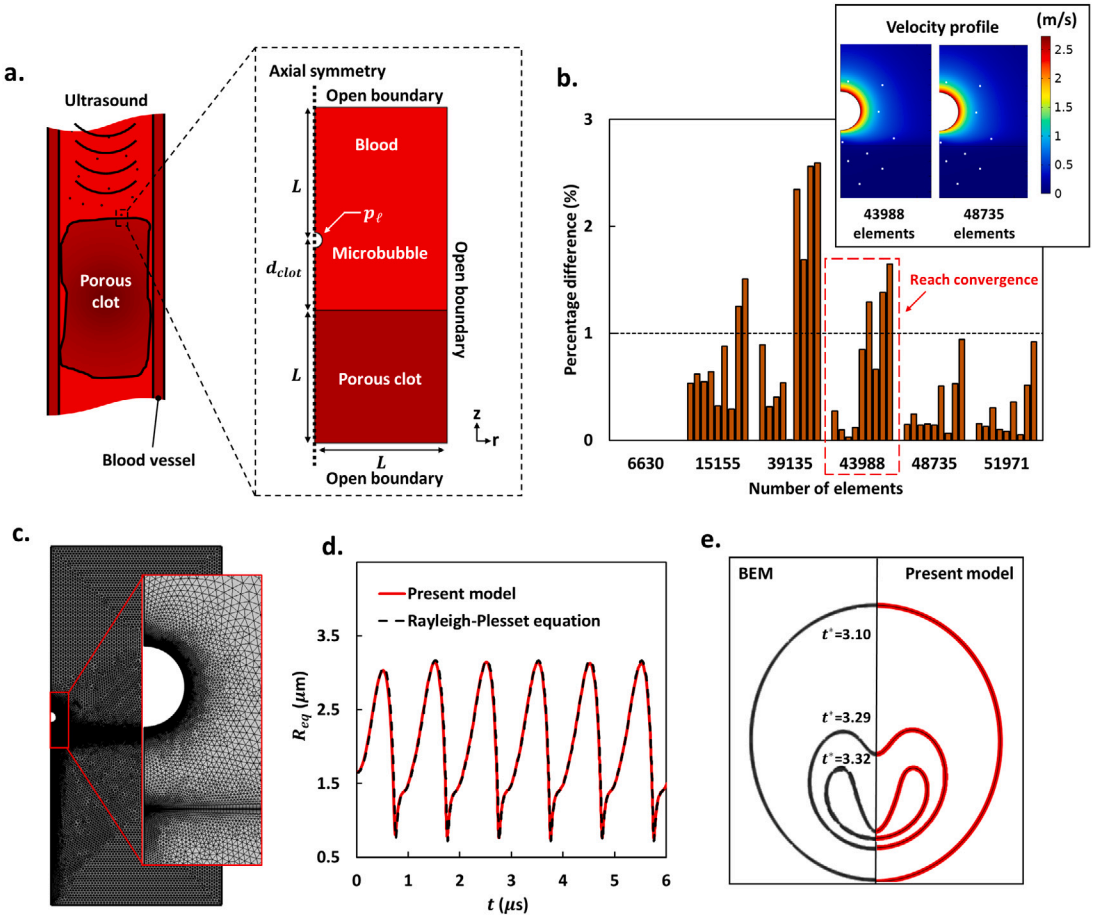

Fig. 2. (a) Model geometry and boundary conditions used in the present study; (b) results of mesh convergence study, where each bar represents the percentage difference in the velocity magnitude at one of the sampled points between two consecutive mesh settings. Inset shows the velocity profile of blood using 43,988 and 48,735 elements. White dots represent the nine sampled points used to determine the percentage difference of blood velocity during the mesh refinement; (c) model discretised using the optimum mesh density; (d) comparison of equilibrium bubble radius between the present model and the Rayleigh–Plesset equation; (e) model validation of jet development using the solution of BEM [25,26]. t^* represents the dimensionless time parameter used in their work.

2.2. Fluid flow model

Ultrasound insonation causes the microbubble to undergo both oscillation and translation [27]. The motion of the microbubble induces flow to the surrounding blood, which can be described using the incompressible Navier–Stokes equations:

$$\rho_\ell \nabla \cdot \boldsymbol{u} = 0, \tag{1}$$

$$\rho_\ell \frac{\partial \boldsymbol{u}}{\partial t} + \rho_\ell (\boldsymbol{u} \cdot \nabla)\boldsymbol{u} = \nabla \cdot \left[-p\boldsymbol{I} + \mu_\ell \left(\nabla \boldsymbol{u} + (\nabla \boldsymbol{u})^T\right)\right], \tag{2}$$

where t (s) is time, $\boldsymbol{u}$ (m/s) is the velocity field describing blood flow, p (Pa) is pressure, $\rho_\ell = 1049$ kg/m^3 [28] is the blood density and μ_ℓ (Pa·s) is the blood dynamic viscosity, which is assumed in this study to be non-Newtonian, such that:

$$\mu_\ell = \mu_\infty + \left(\mu_0 - \mu_\infty\right)\left(1 + (\lambda\dot{\gamma})^2\right)^{\frac{n-1}{2}}, \tag{3}$$

where $\mu_0 = 0.056$ Pa·s and $\mu_\infty = 0.00345$ Pa·s are the viscosity at zero and infinite shear rate, respectively, $\lambda = 3.313$ s is the relaxation time constant, $\dot{\gamma}$ (1/s) is the shear rate and $n = 0.3568$ is a dimensionless parameter [29].

The clot was assumed to be a porous medium [30], such that blood flow inside the clot can be described using the Brinkman equation, which combines the equations for mass and momentum conservation with the Darcy's law for flow in porous media. The viscous transport term is accounted for in Brinkman equation, with both pressure and the velocity field taken as independent of one another. The Brinkman equation is given by [31]:

$$\rho_\ell \nabla \cdot \boldsymbol{u} = 0, \tag{4}$$

$$\begin{aligned}\frac{1}{\varepsilon_p}\rho_\ell \frac{\partial \boldsymbol{u}}{\partial t} + \frac{\rho_\ell}{\varepsilon_p}\left((\boldsymbol{u} \cdot \nabla)\frac{\boldsymbol{u}}{\varepsilon_p}\right) &= -\nabla p + \nabla \cdot \left[\frac{1}{\varepsilon_p}\left(\mu_\ell\left(\nabla \boldsymbol{u} + (\nabla \boldsymbol{u})^T\right) - \frac{2}{3}\mu_\ell (\nabla \cdot \boldsymbol{u})\boldsymbol{I}\right)\right] \\ &\quad - \left(\boldsymbol{\kappa}^{-1}\mu_\ell\right)\boldsymbol{u},\end{aligned} \tag{5}$$

where $\varepsilon_p = 0.4$ and $\boldsymbol{\kappa} = 1 \times 10^{-13}$ m^2 are the porosity and permeability tensor of the clot, respectively [30] . The value of porosity and permeability depends on the clot retraction. Older and retracted clots such as venous thromboses tend to have a lower porosity and permeability compared to fresh and unretracted arterial thromboses [2].

2.3. Bubble dynamics model

In the present study, ultrasound waves were assumed to travel in the -z direction, such that the liquid pressure at the far field can be described using:

$$p_\infty = p_0 - p_A \sin(kz + 2\pi f t), \tag{6}$$

where $p_0 = 100$ kPa is the ambient pressure, p_A (Pa) and f (Hz) are the pressure amplitude and frequency of the ultrasound waves, respectively

and k (1/m) is the wavenumber given by:

$$k = \frac{2\pi f}{c_\ell}, \tag{7}$$

where c_ℓ = 1590 m/s is the speed of sound in blood [28].

The liquid pressure at the bubble surface must obey the pressure continuity condition [22], such that:

$$p_\ell = p_g - p_\sigma - 4\mu_\ell \frac{\dot{R}(t)}{R(t)} - 4\kappa_s \frac{\dot{R}(t)}{R^2(t)} - p_\infty, \tag{8}$$

where p_g (Pa) is the gas pressure inside the bubble, p_σ (Pa) is the Laplace pressure, R (m) is the instantaneous bubble radius, $\dot{R}$ (m/s) is the instantaneous bubble wall velocity and $\kappa_s = 7.5 \times 10^{-9}$ kg/s is the bubble shell viscosity [23]. The third and fourth terms on the right-hand side of Eq. (8) represent the pressure contribution due to the viscosity of surrounding blood and the bubble coating, respectively.

The gas pressure inside the bubble p_g is a function of the microbubble radius, such that [24]:

$$p_g = \left(p_0 + \frac{2\sigma_0}{R_0}\right)\left(\frac{R_0^3 - h^3}{R^3(t) - h^3}\right)^\gamma, \tag{9}$$

where σ_0 = 0.02 N/m is the initial surface tension of the microbubble [23], R_0 (m) is the initial microbubble radius, $h = R_0/5.6$ (m) is the van der Waals core radius of the microbubble and γ = 1.07 is the polytropic index of gas inside the microbubble [24].

During insonation, the microbubble may oscillate in a non-spherical manner depending on the spatial gradient of the blood velocity profile on the bubble surface. In such cases, the use of R to characterise the size of the microbubble is no longer valid. To overcome this, the term R in Eqs (8) and (9) was replaced with the equilibrium bubble radius, R_{eq}, which can be calculated by equating the surface area of the non-spherical bubble to that of a spherical bubble.

The Laplace pressure, which is responsible for the recovery of the spherical shape of the microbubble during oscillation, is given by [22]:

$$p_\sigma = \sigma(R_{eq})K, \tag{10}$$

where K (1/m) is the total curvature of the microbubble and $\sigma(R_{eq})$ (N/m) is the radius dependent surface tension, which can be described using the continuously differentiable form of the Marmottant model [23,32]:

$$\sigma\left(R_{eq}\right) = \sigma_\ell e^{-be^{c\left(1-\frac{R_{eq}\sqrt{1+\frac{\sigma_0}{\chi}}}{R_0}\right)}}, \tag{11}$$

where $\sigma_\ell = 53.45\times10^{-3}$ N/m is the surface tension of blood [33], χ = 0.5 N/m is the bubble shell elasticity [23], and b and c are dimensionless coefficients expressed as:

$$b = -\frac{\ln(\sigma_0/\sigma_\ell)}{e^{c\left(1-\sqrt{1+\frac{\sigma_0}{\chi}}\right)}}, \tag{12}$$

$$c = \frac{2\chi e^1}{\sigma_\ell}\sqrt{1+\frac{\sigma_\ell}{2\chi}}. \tag{13}$$

2.4. Initial–boundary conditions

The microbubble was assumed to be at rest prior to insonation. Therefore, the initial velocity and pressure of blood was set to zero and the ambient pressure, p_0, respectively. To satisfy the velocity continuity condition across the bubble surface, the arbitrary Lagrangian–Eulerian moving mesh algorithm was adopted. This condition sets the instantaneous bubble wall velocity to equal the blood velocity on the microbubble surface, which requires the normal mesh velocity to be equivalent to the normal blood velocity on the bubble surface. On the other hand, the pressure continuity condition across the bubble surface was imposed by using Eq. (8). To evaluate the Laplace pressure in Eq. (10), a weak form of the pressure continuity condition, similar to the one proposed by Hosseinkhah et al. [22], was implemented. Lastly, open boundary conditions were applied to the remaining boundaries of the model, such that:

$$\left[-p\boldsymbol{I} + \mu_\ell\left(\nabla\boldsymbol{u} + (\nabla\boldsymbol{u})^T\right)\right]\boldsymbol{n} = 0, \tag{14}$$

where $\boldsymbol{n}$ is the unit normal vector. Eq. (14) allows blood to either enter or leave the computational domain, depending on the state of oscillation of the microbubble. The boundary conditions implemented in the present study are illustrated in Fig. 2a.

2.5. Numerical implementation

The implementation of the model began with the calculation of liquid pressure at the microbubble surface (see Eq. (8)), which was mainly contributed by pressure variation due to ultrasound waves (see Eq. (6)), the gas pressure inside the microbubble (see Eq. (9)) and the Laplace pressure (see Eq. (10)). The ultrasound waves led to the oscillatory and translational motion of the microbubble, where the resulting blood motion surrounding the microbubble and those within the clot were calculated by solving the fluid flow model (see Section 2.2) along with the initial–boundary conditions (see Section 2.4).

2.6. Mesh convergence

A mesh convergence study was carried out to obtain the mesh setting that results in mesh-independent numerical solutions. The model was primarily discretised into triangular elements except for the interface between the clot and blood, where boundary layer mesh (rectangular elements) were used to improve the estimation of shear stress here. To accurately resolve the curvature of the microbubble during oscillation, a finer mesh size was prescribed on the microbubble surface. The overall element size was then systematically refined and the percentage difference in the blood flow velocity sampled at nine points within the model were determined after every mesh refinement. Specifically, mesh refinement was first performed globally at both the blood and clot domain. This was followed by the local refinement at the blood-clot boundary, and finally at the surface of the microbubble. Fig. 2b presents the results obtained from the mesh convergence study. For a mesh convergence criterion of 1%, it was found that a minimum of 43,988 elements were required to achieve mesh-independent numerical solutions, which can be observed from an almost identical velocity profile when the number of mesh elements was increased further to 48,735 elements. The model discretised using the converged mesh setting is shown in Fig. 2c. The mesh refinement results in element sizes (order of 10^{-6} m) that are much smaller than the minimum wavelength (order of 10^{-3} m) considered in the present study.

During sonothrombolysis, oscillation of the microbubble under both stable and inertial cavitation causes the mesh around the bubble boundary to stretch and distort, which may lead to numerical instabilities. To overcome this problem, an automatic remeshing algorithm was implemented, where re-meshing of the domain was carried out when the element distortion exceeds 0.8, which was sufficient in validating the accuracy of the present model (see Section 2.8).

2.7. Post-collapse flow model

The bubble dynamics model presented in the preceding sections can solve for the oscillation and translation of the microbubble during both stable and inertial cavitation. In the case of inertial cavitation, the microbubble collapses violently to form a high-speed jet, where the top surface of the bubble 'folds' inwards towards the bottom surface. This is illustrated by the green arrows in Fig. 3a. At some point, the top surface will come into contact with the bottom surface, such as shown in the third panel of Fig. 3a. For simplicity, this point is defined as the critical point. Beyond the critical point, the simulation will fail due to the overlapping blood domain and the inability of the present model to form new nodes and mesh connections. This is illustrated in the fourth

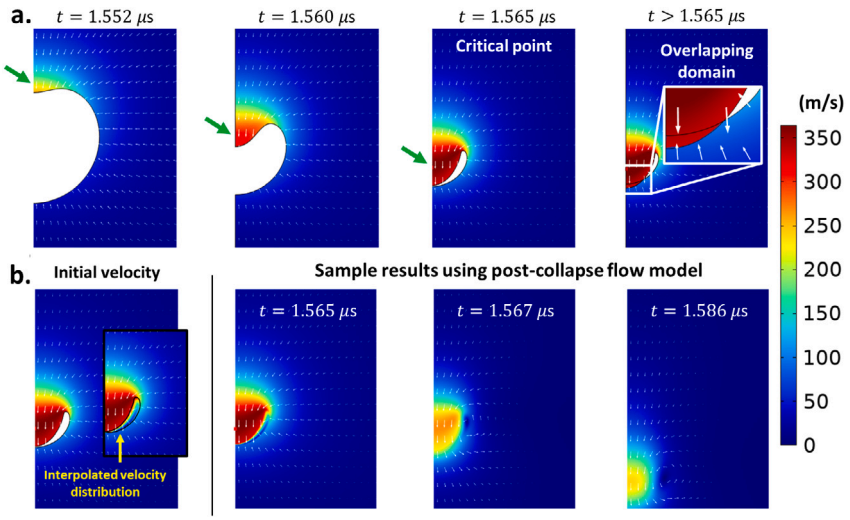

Fig. 3. (a) Velocity profile of blood during the development of high-speed jet; (b) transition of the bubble dynamics model into the post-collapse flow model after the critical point. White arrows represent the velocity vectors of blood. Yellow arrow shows the bubble region, where linear interpolation of the velocity and pressure distribution was carried out based on the surrounding data points.

panel of Fig. 3a. Hence, it is not possible to continue using the same model to simulate the progression of the jet until it impacts the clot surface to estimate the induced shear stress.

To address this, a different model, hereafter known as the post-collapse flow model, was developed to describe the blood flow dynamics beyond the critical point. This model was solved separately after solving the bubble dynamics model, and is meant to be a continuation of the blood flow dynamics after the critical point. Hence, the initial state of the post-collapse flow model, *i.e.*, the initial velocity and pressure fields, were obtained from those of the bubble dynamics model at the critical point. The geometry of the post-collapse flow model was identical to the one used in the bubble dynamics model, except that the presence of the bubble at the critical point (see yellow arrow in Fig. 3b) was neglected and was assumed to be filled with blood. Nevertheless, this assumption created 'empty' data points in the region previously occupied by the bubble, since the bubble dynamics model captures only the field variables in blood. To overcome this, a simple linear interpolation was used to estimate the velocity and pressure distribution across these data points. An example of the interpolated velocity distribution across the region occupied by the bubble at the initial state of the post-collapse flow model is shown in Fig. 3b.

The equations describing the jet progression are given by Eqs (1) and (2) in the blood domain, and Eqs (4) and (5) in the porous clot. The boundary conditions in the post-collapse flow model are identical to the one used in the bubble dynamics model (see Fig. 2a), but without p_ℓ since bubble dynamics was not included. A sample of the simulation results obtained using the post-collapse flow model is illustrated in Fig. 3b, while the corresponding animation is available in the Supplementary Material. The progression of the jet is the result of the initial momentum due to the collapse of the microbubble. As the jet advances, the velocity decreases due to the dissipation of energy and momentum to the surrounding blood [34].

2.8. Model validation

Validation was carried out for both stable and inertial cavitation to ensure the accuracy of the model. For stable cavitation, a microbubble of radius 1.65 μm was exposed to a 200 kPa ultrasound waves at 1.0 MHz frequency. The numerically obtained equilibrium radius, R_{eq} was then compared against the analytical solution obtained by solving the Rayleigh–Plesset equation, as shown in Fig. 2d. One may observe that the present model can accurately reproduce the solution of the Rayleigh–Plesset equation.

The accuracy of the inertial cavitation model was verified against the solution obtained using the BEM. For this purpose, the model was modified to mimic the settings used in the study by Mobadersany and Sarkar [25], namely (i) an inviscid fluid ($\mu_\ell = 0$ Pa s) surrounding the microbubble, (ii) negligible bubble shell viscosity ($\kappa_s = 0$), (iii) use of the exponential elasticity model [35] instead of the Marmottant model, (iv) a rigid wall with no-slip boundary condition instead of a porous clot, (v) a spatially uniform p_∞ at the bubble surface ($kz = 0$ in Eq. (6)), and (vi) adjusted model parameters to match those used by Mobadersany and Sarkar [25]. The bubble shapes during the jet development at three different dimensionless times, t^* are shown in Fig. 2e, where good agreement between the present model and the BEM is observed.

3. Results

The effects of ultrasound and microbubble parameters on the dynamics of stable and inertial cavitation during sonothrombolysis were investigated separately. For stable cavitation, only the effects of microbubble radius and ultrasound frequency were examined. This is because stable cavitation is conditioned upon a low ultrasound pressure amplitude. For inertial cavitation, the effects of ultrasound frequency and pressure amplitude, and the microbubble radius were investigated. Several outputs that help to explain the outcome of sonothrombolysis were considered. These include the equilibrium bubble radius R_{eq}, bubble wall velocity (temporal gradient of R_{eq}), the distance travelled by the microbubble, the velocity and size of the high-speed jet (only for inertial cavitation), and the magnitude of shear stress induced on the clot surface, which can be estimated using $\tau_{rz} = \mu_\ell \left(\frac{\partial u}{\partial z} + \frac{\partial w}{\partial r}\right)$, where u (m/s) and w (m/s) are the r- and z- components of the velocity field, respectively. In general, a higher shear stress on the clot surface translates to more stretching of the pores on the clot surface (for stable cavitation) and more intense erosion of the clot (for inertial cavitation), both of which improves the penetration of drugs into the clot to enhance outcome of sonothrombolysis.

3.1. Stable cavitation

3.1.1. Effects of microbubble radius, R_0

The effects of microbubble radius were investigated for $R_0 = 0.55$, 1.10, 1.65 μm, which represents the mean bubble radii used in typical experimental studies of sonothrombolysis [4]. The ultrasound frequency was set to $f = 0.5$ MHz [6], while a low pressure amplitude

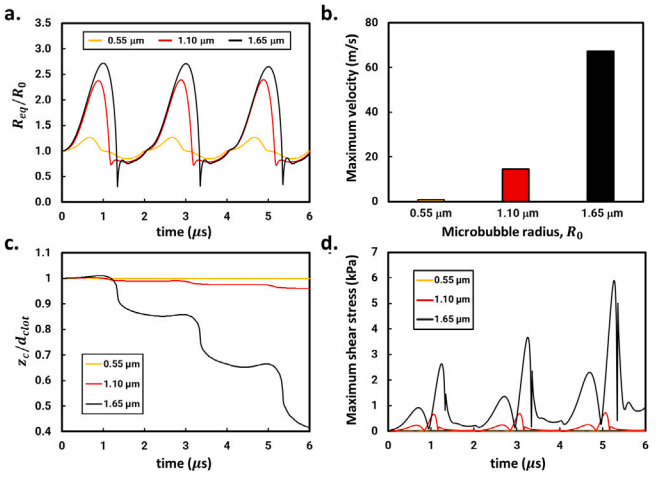

Fig. 4. Effects of microbubble radius R_0 on: (a) the instantaneous equilibrium bubble radius R_{eq} normalised against R_0, (b) the maximum bubble wall velocity, (c) the normalised distance between microbubble and clot surface z_c/d_{clot}, and (d) the maximum shear stress on the clot surface. Ultrasound pressure amplitude and frequency were 200 kPa and 0.5 MHz, respectively.

of p_A = 200 kPa (decided following a preliminary study) was applied to ensure stable cavitation. Fig. 4a plots the normalised instantaneous microbubble equilibrium radius R_{eq} against time for the three values of R_0 considered. Larger microbubbles oscillate at a greater amplitude than smaller ones, although the differences in the degree of oscillation diminishes with increasing microbubble radius. Larger microbubbles also oscillate at a higher velocity, as indicated by the plot of the maximum bubble wall velocity in Fig. 4b. Fig. 4c plots the transient z-coordinate of the bubble centre (z_c) normalised against the standoff distance, d_{clot}, *i.e.*, z_c/d_{clot}. A smaller z_c/d_{clot} implies that the microbubble has traversed closer to the clot surface. From Fig. 4c, the farthest distance travelled was observed for the microbubble with R_0 = 1.65 μm, while microbubbles with R_0 = 0.55 and 1.10 μm barely travelled from its original position.

Fig. 5 illustrates the velocity profile of the R_0 = 1.65 μm microbubble during the contraction phase of the third acoustic cycle. An animation of the microbubble oscillation is available in the Supplementary Material. The microbubble oscillated asymmetrically with a higher velocity magnitude across the top surface. This resulted in a downward movement of the microbubble towards the clot as a consequence of a greater net force across the top surface. This explains the greater distance travelled by the microbubble (see Fig. 4c). The microbubble also demonstrated a tendency to transition towards inertial cavitation, as evident by the partial formation of jet that did not penetrate the lower surface of the microbubble. In contrast, for microbubbles with R_0 = 0.55 and 1.10 μm, the velocity profile surrounding the blood during the contraction phase is almost symmetrical (see Supplementary Material), resulting in an almost uniform hydrodynamic force around the microbubbles that reduced their translational motion.

To understand how the bubble dynamics affect the clot surface, the maximum flow-induced shear stress on the clot surface was estimated and their values plotted against time are shown in Fig. 4d. The largest microbubble induced the greatest shear stress on the clot surface, which may be explained by the higher bubble wall velocity and the proximity of the microbubble (greater translational distance) to the clot surface. The latter is demonstrable by the increasing peak shear stress (see Fig. 4d) as the microbubble moves closer to the clot (see Fig. 4c). Overall, the shear stress due to the oscillation of the R_0 = 1.65 μm microbubble was one to three orders of magnitude greater than those induced by the R_0 = 0.55 and 1.10 μm microbubbles. These findings suggest that larger microbubbles produce better sonothrombolytic outcome during stable cavitation.

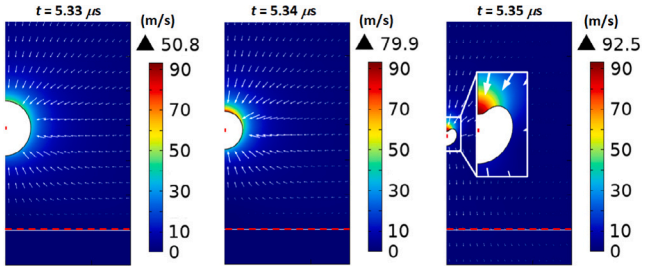

Fig. 5. Velocity profile of blood during contraction phase for microbubble of R_0 = 1.65 μm. Dashed red lines represent the clot surface. White arrows represent the velocity vectors of blood. Inset: enlarged view of the asymmetric bubble shape that represents the partial formation of jet.

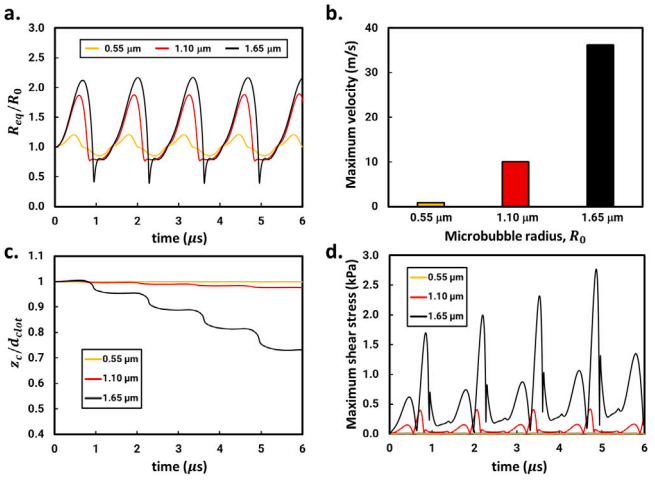

Fig. 6. Effects of microbubble radius R_0 on: (a) the instantaneous equilibrium bubble radius R_{eq} normalised against R_0, (b) the maximum bubble wall velocity, (c) the normalised distance between microbubble and clot surface z_c/d_{clot}, and (d) the maximum shear stress on the clot surface. Ultrasound pressure amplitude and frequency were 200 kPa and 0.75 MHz, respectively.

3.1.2. *Effects of ultrasound frequency, f*

The effects of ultrasound frequency on the bubble dynamics during stable cavitation were investigated by increasing f to 0.75 MHz [15], and simulations were repeated for the three bubble radii (R_0 = 0.55, 1.10, 1.65 μm) and ultrasound pressure amplitude (p_A = 200 kPa) considered in Section 3.1.1. The results obtained are presented in Fig. 6. Increasing the ultrasound frequency led to smaller oscillation amplitude but with more frequent oscillations (compare Figs. 4a and 6a). The decrease in oscillation amplitude resulted in a slower bubble wall velocity (compare Figs. 4b and 6b). Microbubbles oscillating at a higher frequency also travelled shorter distances than those oscillating at a lower frequency (compare Figs. 4c and 6c). As a result, the flow-induced shear stress on the clot surface was significantly lower at higher ultrasound frequency (compare Figs. 4d and 6d). An important parameter during cavitation is the mechanical index (MI), which measures the ultrasound's bioeffects. A lower MI value implies a decrease in the potential for cavitation. The MI can be estimated from the ratio of the peak negative pressure (MPa) to the square root of ultrasound frequency (MHz). For the 0.5 and 0.75 MHz ultrasound at 200 kPa, the MI values were calculated to be 0.28 and 0.23, respectively. This suggests that increasing the ultrasound frequency, which reduces the MI, may not be ideal for sonothrombolysis, as the microbubbles tend to undergo stable cavitation only.

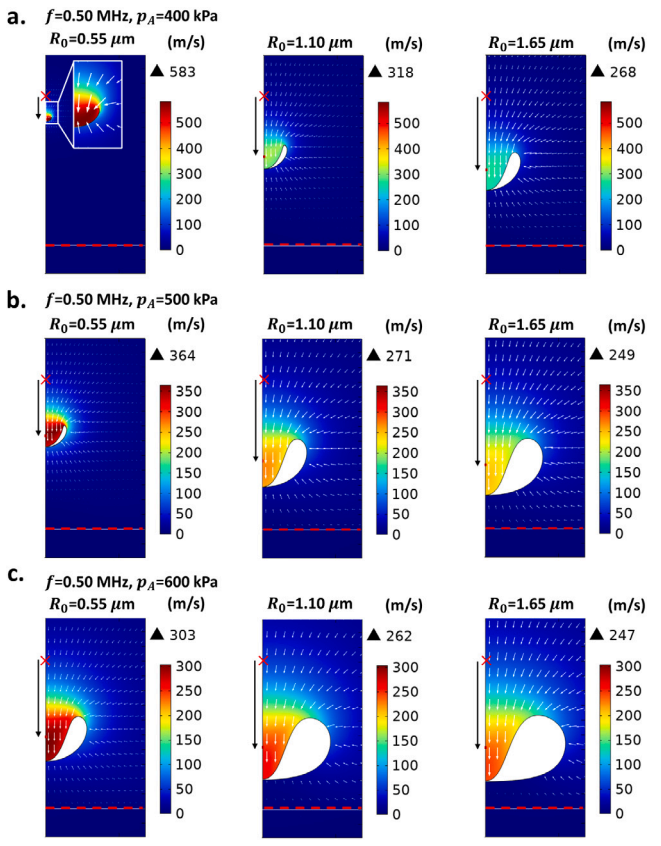

Fig. 7. Velocity profile of blood at the critical point using microbubble of R_0 = 0.55, 1.10, and 1.65 μm at (a) p_A = 400 kPa, (b) p_A = 500 kPa, and (c) p_A = 600 kPa, using ultrasound frequency f = 0.5 MHz. Dashed red lines represent the clot surface. White arrows are the velocity vectors of blood. Black arrows represent the distance travelled by microbubbles. The initial position of bubble centre is marked by red crosses. Inset: enlarged view of the jet.

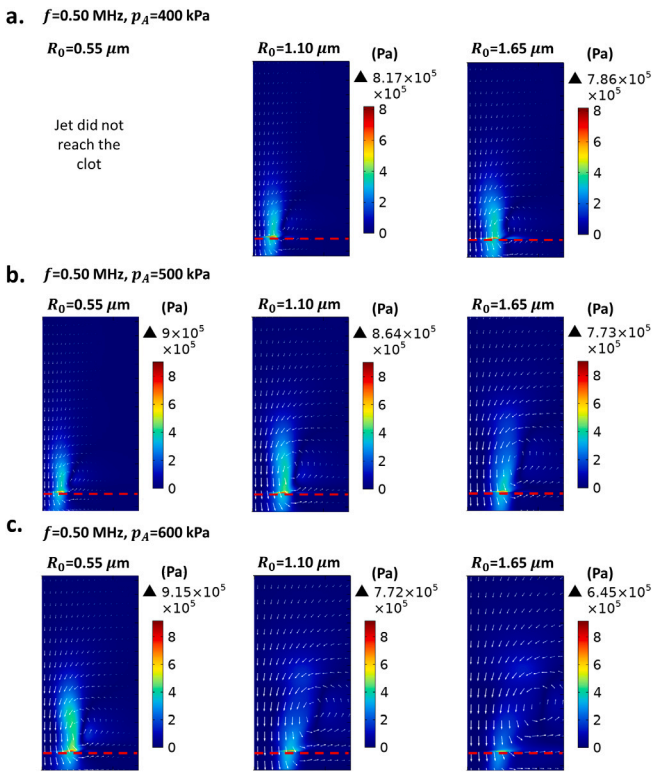

Fig. 8. Shear stress distribution during the maximum shear stress using microbubble of R_0 = 0.55, 1.10, and 1.65 μm at (a) p_A = 400 kPa, (b) p_A = 500 kPa, and (c) p_A = 600 kPa, using ultrasound frequency f = 0.5 MHz. Dashed red lines represent the clot surface. White arrows are the velocity vectors of blood.

3.2. Inertial cavitation

3.2.1. Effects of microbubble radius, R_0

Similar to the study on stable cavitation (see Section 3.1.1), the effects of microbubble radius during inertial cavitation were examined for R_0 = 0.55, 1.10, and 1.65 μm. Ultrasound pressure amplitude and frequency were set to p_A = 400 kPa and f = 0.5 MHz, respectively. The higher pressure amplitude was necessary to ensure the microbubbles undergo inertial cavitation. Contours of the velocity profile at the critical point, *i.e.*, the point just before the microbubble splits, are illustrated in Fig. 7a for each of the microbubble radius considered. The presence of the high-speed jet, which is characteristic of microbubbles undergoing inertial cavitation, can be visualised from the region in dark red, *i.e.*, the region with the highest velocity, while values of the maximum jet velocity are summarised in Table 1. Smaller microbubbles collapse at a higher velocity than larger ones, with the higher jet velocity suggesting a greater mechanical impact on the clot surface.

The distance travelled by the microbubble from the start of insonation to the critical point is depicted by the black arrows in Fig. 7a, where the initial position of the microbubble centre is marked by the red cross. Values of the distance travelled by the microbubble are presented in Table 1. Larger microbubbles tend to move closer towards the clot before reaching the critical point. The proximity of the microbubble to the clot enhances the mechanical impact of the jet on the clot surface, which is beneficial for sonothrombolysis. However, larger microbubbles also collapse at a lower velocity and this can be detrimental to the sonothrombolytic effect. Herein lies a competing effect between the distance travelled by the microbubble and the jet velocity for a given microbubble radius. While larger microbubbles can traverse closer to the clot, its benefit could potentially be negated by the slower jet velocity.

To understand which effect is more important during sonothrombolysis, the post-collapse flow model developed in Section 2.7 was employed to estimate the dynamics of blood flow beyond the critical point and subsequently the induced shear stress on the clot surface. The magnitude of the maximum jet induced shear stress on the clot surface is presented in Table 1, and the corresponding shear stress distribution is illustrated in Fig. 8a. Note that the shear stress values were higher in Fig. 8 compared to Table 1, as the former corresponds to shear stress in blood domain just before the clot surface, while the latter represent the shear stress on the clot surface. Although the 0.55 μm microbubble had the highest jet velocity, the small jet size meant that it possessed very low momentum to carry the jet towards the clot surface. Consequently, most of the energy and momentum dissipated into the surrounding blood and the jet diminished before reaching the clot. In contrast, microbubbles with R_o = 1.10 and 1.65 μm demonstrated significantly larger shear stress on the clot surface (≈ 600 kPa). This suggests that the proximity of the microbubble (and hence the jet) to the clot surface is more important than the magnitude of jet velocity in enhancing the sonothrombolytic effect. These findings indicate that microbubbles with R_o = 1.10 and 1.65 μm undergoing inertial cavitation would be the better choice for sonothrombolysis.

3.2.2. Effects of ultrasound pressure, p_A

The effects of ultrasound pressure amplitude were investigated by increasing p_A to 500 kPa and simulations were repeated for the three bubble radii (0.55, 1.1 and 1.65 μm) and ultrasound frequency (0.5 MHz) considered in Section 3.2.1. Contours of the velocity surrounding the microbubble at the critical point are illustrated in Fig. 7b, while values of the maximum jet velocity and the distance travelled by the

Table 1
Effects of p_A on the values of the maximum jet velocity, distance travelled by the microbubble and the maximum shear stress magnitude obtained for R_0 = 0.55, 1.10, and 1.65 μm, at f = 0.50 MHz.

Parameter	p_A = 400 kPa			p_A = 500 kPa			p_A = 600 kPa		
	R_o (μm)			R_o (μm)			R_o (μm)		
	0.55	1.10	1.65	0.55	1.10	1.65	0.55	1.10	1.65
Maximum jet velocity (m/s)	583	318	268	364	271	249	303	262	247
Distance travelled (μm)	1.44	3.93	4.85	3.65	5.32	5.66	5.12	5.77	5.85
Maximum shear stress (kPa)	†	593	583	650	629	571	673	573	479

†Not applicable.

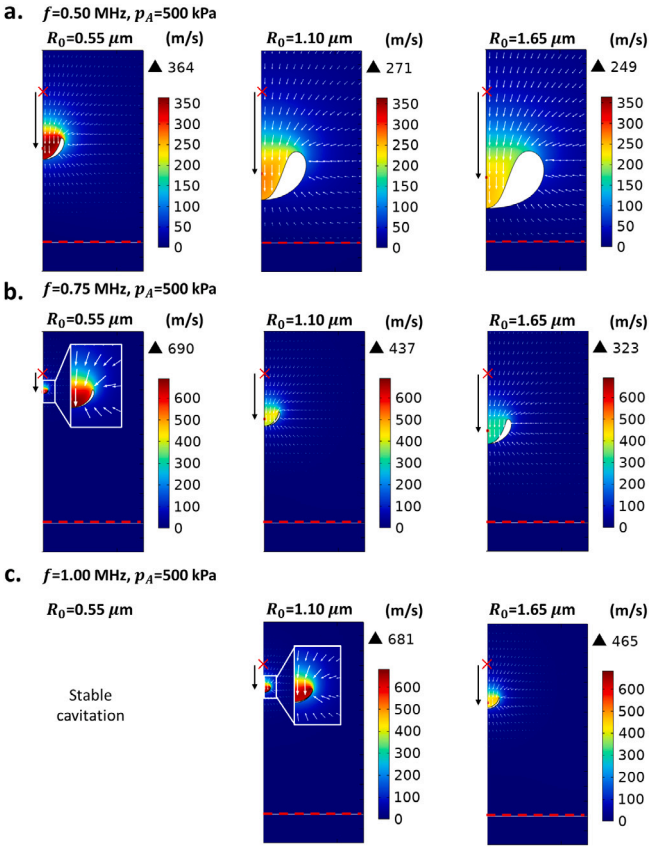

Fig. 9. Velocity profile of blood at the critical point using microbubble of R_0 = 0.55, 1.10, and 1.65 μm at (a) f = 0.50 MHz, (b) f = 0.75 MHz, and (c) f = 1.00 MHz, using ultrasound pressure p_A = 500 kPa. Dashed red lines represent the clot surface. White arrows are the velocity vectors of blood. Black arrows represent the distance travelled by microbubbles. The initial position of bubble centre is marked by red crosses. Inset: enlarged view of the jet.

microbubble are summarised in Table 1. For a given microbubble radius, a higher ultrasound pressure led to the formation of a larger jet and a greater distance travelled by the microbubble, although the jet velocity decreased. From Table 1 and Fig. 8b, it is evident that increasing the pressure amplitude to 500 kPa can elevate the shear stress induced on the clot surface by the 0.55 and 1.10 μm microbubbles. Since the jet velocity decreases with increasing pressure amplitude, the increase in shear stress with pressure amplitude is likely due to the proximity of the microbubbles to the clot surface as a result of the greater distance travelled at p_A = 500 kPa. Interestingly, a decrease in shear stress was observed for the 1.65 μm microbubble. This suggests that the reduced jet velocity can eventually lower the impact of the jet even when the microbubble is sufficiently close to the clot. A similar observation was obtained when increasing the pressure to p_A = 600 kPa (see Table 1, Fig. 7c, and Fig. 8c). Therefore, both the jet velocity and translational distance are critical in enhancing the sonothrombolytic effect.

3.2.3. *Effects of ultrasound frequency, f*

The ultrasound frequency was increased from 0.5 MHz to 0.75 MHz and simulations were repeated for the three bubble radii (0.55, 1.1 and 1.65 μm) and ultrasound pressure amplitude (500 kPa) considered in Section 3.2.2. The corresponding velocity profiles of blood at the critical point are presented in Fig. 9b, where Fig. 9a are reproduced from Fig. 7b to facilitate visual comparison. Table 2 summarises the values of the maximum jet velocity, the distance travelled by the microbubble and the maximum shear stress on the clot surface. Contours of the maximum shear stress on the clot surface may be found in the Supplementary Material. Increasing the ultrasound frequency led to a higher jet velocity, but a smaller jet and a shorter distance travelled by the microbubble. The short distance travelled by the 0.55 and 1.1 μm microbubble implies that the microbubble is far from the clot surface such that the jet momentum dissipated to the surrounding blood before impinging the clot surface. On the contrary, the 1.65 μm microbubble generated larger shear stress at higher ultrasound frequency, suggesting that the increased jet velocity in this case outweighed the shorter distance travelled by the microbubble. Hence, the selection of the suitable microbubble radius depends greatly on the ultrasound frequency.

At higher frequency of f = 1 MHz, the oscillation of 0.55 μm microbubble became stable and no formation of jet was observed. Although high-speed jet was observed in 1.10 μm microbubble, the jet did not reach the clot due to the short translational distance. Similarly, the short translational distance of 1.65 μm at f = 1 MHz only enabled the jet to barely hit the clot, resulting in a low shear stress of only 32 kPa. This result indicates that a low frequency ultrasound is generally more advantageous for increasing the effect of inertial cavitation during sonothrombolysis.

4. Discussions

Results from the present study demonstrated that larger microbubbles insonated at a lower frequency are ideal during stable cavitation for elevating the shear stress on the clot surface and ultimately improve the sonothrombolytic effect. However, the selection of an optimum combination of parameters for microbubbles undergoing inertial cavitation is not straightforward. From the results presented in Section 3.2, it was not possible to determine whether larger microbubbles, higher ultrasound pressure or lower ultrasound frequency are ideal for sonothrombolysis, since their effects on shear stress at the clot surface depend greatly on their interaction.

From Tables 1 and 2, one may deduce that jet velocity and distance travelled by the microbubble are governed by the microbubble radius, pressure amplitude and frequency. An increase in jet velocity is always accompanied by a decrease in the distance travelled by the microbubble and vice versa; suggesting a tug-of-war scenario, where the beneficial impact of higher jet velocity is always competing with the detrimental effect of a shorter distance travelled. This is unfavourable to the shear stress when there is a considerable decrease in the translational

Table 2
Effects of f on the values of the maximum jet velocity, distance travelled by the microbubble and the maximum shear stress magnitude obtained for R_0 = 0.55, 1.10, and 1.65 μm, at p_A = 500 kPa.

Parameter	f = 0.50 MHz			f = 0.75 MHz			f = 1.00 MHz		
	R_o (μm)			R_o (μm)			R_o (μm)		
	0.55	1.10	1.65	0.55	1.10	1.65	0.55	1.10	1.65
Maximum jet velocity (m/s)	364	271	249	690	437	323	†	681	465
Distance travelled (μm)	3.65	5.32	5.66	1.13	2.97	3.80	†	1.63	2.37
Maximum shear stress (kPa)	650	629	571	†	251	581	†	†	32

†Not applicable.

distance or the jet velocity, following an increase in the value of their counterpart. As such, one may hypothesise that the maximum shear stress is attainable only when an equilibrium between the sonothrombolytic effect of jet velocity and translational distance is achieved. From Table 1, the largest shear stress was obtained for the R_0 = 0.55 μm microbubble insonated with f = 0.50 MHz and p_A = 600 kPa. However, neither the jet velocity nor the distance travelled by the microbubble were at their maximum, which lends further credence to the aforementioned hypothesis. The increase in shear stress due to the insonation of smaller microbubbles at a certain ultrasound pressure amplitude and frequency may explain the improvement in sonothrombolysis when using nanodroplets instead of microbubbles, as demonstrated recently [36].

Although the insonation of a microbubble with R_0 = 0.55 μm at f = 0.50 MHz and p_A = 600 kPa yielded the maximum shear stress, this finding must be interpreted with caution as the bubble dynamics is also affected by the type of microbubble (*i.e.*, different shell elasticity and viscosity), the clot permeability and the different ultrasound administration methods. Therefore, it may not be straightforward to ascertain the right balance between the jet velocity and the distance travelled by the microbubble during actual sonothrombolysis. A potential solution to this is to overcome the competing effect so that a high jet velocity can happen without sacrificing the distance between the jet and the clot surface. This is theoretically possible by positioning the microbubble closer to the clot surface prior to insonation. Unfortunately, this is not something that can be controlled during the treatment. Therefore, a more reliable way is to increase the translational distance of the microbubble towards the clot prior to the jet formation. Although this can be achieved by either lowering the ultrasound frequency, increasing the ultrasound pressure or using a large microbubble (see Tables 1 and 2), doing so also reduces the jet velocity and weaken the shear stress on the clot surface.

An attractive alternative to increase the translational distance is to insonate the microbubbles so that they are about to undergo inertial cavitation (see Section 3.1.1). Unlike the fully developed jet during inertial cavitation that splits the microbubble, the partially developed jet enables the microbubble to travel closer towards the clot due to the net downward force (see Fig. 5 and animation in Supplementary Material), while preserving the lifespan of the microbubble. This can be accomplished by first insonating the microbubble using low amplitude ultrasound to allow it to travel close to the clot, before the amplitude is raised to induce inertial cavitation and hence, complete the development of the jet. This is open for future investigations.

Recently, Tan et al. [37] developed a macroscale model to investigate the performance of sonothrombolysis using a forward-viewing intravascular ultrasound transducer under various conditions and operating parameters. Smaller microbubbles were found to be better for sonothrombolysis due to weaker acoustic attenuation, which allows a larger pressure magnitude to reach the clot surface. Their findings support the results from the present study, where smaller microbubbles produce higher shear stress on the clot surface when paired with the correct combination of frequency and pressure. A higher pressure is also better for sonothrombolysis as it overcomes the attenuation from the microbubbles [37]. This contradicted the present study, where a higher pressure may reduce the shear stress on the clot surface due to the slower jet velocity (see Table 1). This emphasises the importance of considering both the macroscale and microscale effects to elucidate the complete understanding on the parameter interaction during sonothrombolysis.

There are a few limitations that must be acknowledged for further improvements in future investigations. Firstly, the model was developed in the 2D axisymmetric coordinate system, which allowed the ultrasound waves to only travel along the z-axis (*i.e.*, the direction parallel to the axis of symmetry). Consequently, the translation of the microbubble and the direction of high-speed jet are restricted to the z-direction. In the actual case, the direction of the ultrasound waves may not necessary be perpendicular to the surface of the clot. Therefore, future study should consider a full 3D model to better represent the conditions of the treatment, although it must be pointed out that doing so will require substantial computational resources.

Secondly, the present study focused on elucidating the fundamental understanding on the biomechanical interaction between one microbubble and the clot surface. In the actual case, multiple microbubbles may be present around the clot and the re-radiated pressure field from the neighbouring microbubbles may influence the dynamics of the microbubble [24]. Interaction forces exist between the microbubbles, which can either be attractive or repulsive [38]. It has also been reported that the high-speed jet tends to point towards the neighbouring microbubble [39], which may reduce or completely render the effect of jet useless for sonothrombolysis. Therefore, consideration of multiple microbubbles is necessary in future studies to provide a more realistic visualisation of acoustic cavitation during the actual treatment. Nevertheless, the main challenge associated with the simulation of multiple bubbles is the need of a computationally expensive 3D model to account for the presence of microbubbles at various locations.

Thirdly, blood was assumed to be incompressible, which can be problematic when the jet velocity becomes comparable to the speed of sound in blood, which is approximately 1590 m/s [28]. This was not an issue in the present study since all the high-speed jets formed during the first oscillation cycle, where compressibility may not have been significant [40]. Nevertheless, the compressibility effect may still be important as it accounts for the substantial energy loss of the microbubble at the end of the collapse [40]. Therefore, future work should consider incorporating the compressibility effect in order to generalise the application of the current model to higher jet velocity and jets that are formed after multiple oscillation cycles. Lastly, the present model did not consider the structural deformation of the clot due to the hydrodynamic forces imparted by the microbubble oscillation. In addition to being a porous material, blood clot is known for its viscoelasticity [41,42] and hyperelasticity [43]. There are a large number of models that describe the structural properties of clot. However, the values of these properties depend greatly on the loading configuration, the magnitude of loading, the rate of loading and even the type of the model that is used to fit the deformation data [44]. In addition, most of the existing structural models have not considered the porous nature of the clot, which makes them inappropriate to be coupled with the present model. For these reasons, computational modelling of the clot deformation during sonothrombolysis remains a challenge to be addressed.

5. Conclusions

The present study was carried out in an effort to identify how ultrasound and microbubble parameters affect the outcome of sonothrombolysis. Using a computational model developed specifically for this purpose, simulations were carried out for a microbubble undergoing stable and inertial cavitation during sonothrombolysis treatment. During stable cavitation, the insonation of a large microbubble at low ultrasound frequency induced the highest shear stress on the clot surface, which enhances the sonothrombolytic effect. This was found to be due to the greater distance travelled by the microbubble towards the clot. On the other hand, the selection of the suitable parameters is not as intuitive for inertial cavitation, since their effects on elevating the shear stress depend greatly on the interaction with each other. Moreover, a strong competing effect was uncovered between the jet velocity and the distance travelled by the microbubble during inertial cavitation. In this case, a right balance between the jet velocity and the translational distance is of paramount importance to maximise the shear stress on the clot surface. The ability of the computational model to visualise the bubble behaviour helps to establish a better understanding of the roles and contributions of stable and inertial cavitation during sonothrombolysis. The results from the present study open opportunities for the future optimisation of the treatment, thus paving the way for actual clinical implementation of sonothrombolysis.

Funding

None

CRediT authorship contribution statement

Zhi Qi Tan: Formal analysis, Investigation, Methodology, Validation, Writing – original draft. **Ean Hin Ooi:** Conceptualization, Formal analysis, Project administration, Supervision, Writing – review & editing. **Yeong Shiong Chiew:** Writing – review & editing, Data curation, Methodology, Supervision. **Ji Jinn Foo:** Investigation, Supervision, Writing – review & editing. **Yin Kwee Ng:** Resources, Software, Supervision, Writing – review & editing. **Ean Tat Ooi:** Conceptualization, Investigation, Supervision, Writing – review & editing.

Declaration of competing interest

The authors declare that they have no known competing financial interests or personal relationships that could have appeared to influence the work reported in this paper.

Appendix A. Supplementary data

Supplementary material related to this article can be found online at https://doi.org/10.1016/j.bbe.2024.04.003.

References

[1] Xu S, Zong Y, Feng Y, Liu R, Liu X, Hu Y, et al. Dependence of pulsed focused ultrasound induced thrombolysis on duty cycle and cavitation bubble size distribution. Ultrason Sonochemistry 2015;22:160–6.
[2] Goel L, Jiang X. Advances in sonothrombolysis techniques using piezoelectric transducers. Sensors 2020;20:1288.
[3] Guo S, Du X, Wang X, Lu S, Shi A, Xu S, et al. Reduced clot debris size using standing waves formed via high intensity focused ultrasound. Appl Phys Lett 2017;111:123701.
[4] Wu J, Xie F, Kumar T, Liu J, Lof J, Shi W, et al. Improved sonothrombolysis from a modified diagnostic transducer delivering impulses containing a longer pulse duration. Ultrasound Med Biol 2014;40:1545–53.
[5] Xie F, Lof J, Everbach C, He A, Bennett RM, Matsunaga T, et al. Treatment of acute intravascular thrombi with diagnostic ultrasound and intravenous microbubbles. J Am Coll Cardiol Cardiovasc Imaging 2009;2:511–8.
[6] Goel L, Wu H, Kim H, Zhang B, Kim J, Dayton PA, et al. Examining the influence of low-dose tissue plasminogen activator on microbubble-mediated forward-viewing intravascular sonothrombolysis. Ultrasound Med Biol 2020;46:1698–706.
[7] Kim H, Kim J, Wu H, Zhang B, Dayton PA, Jiang X. A multi-pillar piezoelectric stack transducer for nanodroplet mediated intravascular sonothrombolysis. Ultrasonics 2021;116:106520.
[8] Bader KB, Bouchoux G, Holland CK. Sonothrombolysis. Therapeutic Ultrasound 2016;880:339–62.
[9] Weiss HL, Selvaraj P, Okita K, Matsumoto Y, Voie A, Hoelscher T, et al. Mechanical clot damage from cavitation during sonothrombolysis. J Acoust Soc Am 2013;133:3159–75.
[10] Chen X, Leeman JE, Wang J, Pacella JJ, Villanueva FS. New insights into mechanisms of sonothrombolysis using ultra-high-speed imaging. Ultrasound Med Biol 2014;40:258–62.
[11] Datta S, Coussios C, Ammi AY, Mast TD, de Courten-Myers GM, HollandK CK. Ultrasound-enhanced thrombolysis using definity® as a cavitation nucleation agent. Ultrasound Med Biol 2008;34:1421–33.
[12] Kim J, Lindsey BD, Chang WY, Dai X, Stavas JM, Dayton PA, et al. Intravascular forward-looking ultrasound transducers for microbubble-mediated sonothrombolysis. Sci Rep 2017;7:1–10.
[13] Borrelli MJ, O'Brien Jr WD, Hamilton E, Oelze ML, Wu J, Bernock LJ, et al. Influences of microbubble diameter and ultrasonic parameters on in vitro sonothrombolysis efficacy. J Vascular Intervent Radiol 2012;23:1677–84.
[14] Zhang B, Wu H, Kim H, Welch PJ, Cornett A, Stocker G, et al. A model of high-speed endovascular sonothrombolysis with vortex ultrasound-induced shear stress to treat cerebral venous sinus thrombosis. Research 2023;6:0048.
[15] Goel L, Wu H, Zhang B, Kim J, Dayton PA, Xu Z, et al. Safety evaluation of a forward-viewing intravascular transducer for sonothrombolysis: an in vitro and ex vivo study. Ultrasound Med Biol 2021;47:3231–9.
[16] Petit B, Yan F, Tranquart F, Allémann E. Microbubbles and ultrasound-mediated thrombolysis: a review of recent in vitro studies. J Drug Deliv Sci Technol 2012;22:381–92.
[17] Xie Y, Hu J, Lei W, Qian S. Prediction of vascular injury by cavitation microbubbles in a focused ultrasound field. Ultrason Sonochemistry 2022;88:106103.
[18] Zeng Q, An H, Ohl CD. Wall shear stress from jetting cavitation bubbles: Influence of the stand-off distance and liquid viscosity. J Fluid Mech 2022;932:A14.
[19] Wang S, Zhang A, Liu Y, Zeng D. Numerical simulation of bubble dynamics in an elastic vessel. Eur Phys J E 2013;36:119.
[20] Hosseinkhah N, Goertz DE, Hynynen K. Microbubbles and blood–brain barrier opening: a numerical study on acoustic emissions and wall stress predictions. IEEE Trans Biomed Eng 2014;62:1293–304.
[21] Khodabakhshi Z, Hosseinkhah N, Ghadiri H. Pulsating microbubble in a microvessel and mechanical effect on vessel wall: a simulation study. J Biomed Phys Eng 2021;11:629–40.
[22] Hosseinkhah N, Chen H, Matula TJ, Burns PN, Hynynen K. Mechanisms of microbubble–vessel interactions and induced stresses: A numerical study. J Acoust Soc Am 2013;134:1875–85.
[23] Gümmer J, Schenke S, Denner F. Modelling lipid-coated microbubbles in focused ultrasound applications at subresonance frequencies. Ultrasound Med Biol 2021;47:2958–79.
[24] Qin D, Zou Q, Lei S, Wang W, Li Z. Cavitation dynamics and inertial cavitation threshold of lipid coated microbubbles in viscoelastic media with bubble–bubble interactions. Micromachines 2021;12:1125.
[25] Mobadersany N, Sarkar K. The dynamic of contrast agent and surrounding fluid in the vicinity of a wall for sonoporation. In: Katz J, editor. 10th international symposium on cavitation - CAV2018. Baltimore, Maryland, USA: ASME Press; 2018, p. 257–62.
[26] Mobadersany N, Sarkar K. The dynamic of contrast agent and surrounding fluid in the vicinity of a wall for sonoporation. 2018, arXiv preprint arXiv:1802.08652.
[27] Acconcia C, Leung BYC, Hynynen K, Goertz DE. Interactions between ultrasound stimulated microbubbles and fibrin clots. Appl Phys Lett 2013;103:053701.
[28] Treeby BE, Zhang EZ, Thomas AS, Cox BT. Measurement of the ultrasound attenuation and dispersion in whole human blood and its components from 0-70 MHz. Ultrasound Med Biol 2011;37:289–300.
[29] Husain I, Labropulu F, Langdon C, Schwark J. A comparison of Newtonian and non-Newtonian models for pulsatile blood flow simulations. J Mech Behav Mater 2013;21:147–53.
[30] Xu S, Xu Z, Kim OV, Litvinov RI, Weisel JW, Alber M. Model predictions of deformation, embolization and permeability of partially obstructive blood clots under variable shear flow. J R Soc Interface 2017;14:20170441.
[31] Nield DA, Bejan A. Convection in porous media, vol. 3, New York: Springer; 2006.
[32] Marmottant P, Van Der Meer S, Emmer M, Versluis M, De Jong N, Hilgenfeldt S, et al. A model for large amplitude oscillations of coated bubbles accounting for buckling and rupture. J Acoust Soc Am 2005;118:3499–505.

[33] Yadav SS, Sikarwar BS, Ranjan P, Janardhanan R, Goyal A. Surface tension measurement of normal human blood samples by pendant drop method. J Med Eng Technol 2020;44:227–36.
[34] Brujan EA. Jets from pulsed-ultrasound-induced cavitation bubbles near a rigid boundary. J Phys D: Appl Phys 2017;50:215302.
[35] Paul S, Katiyar A, Sarkar K, Chatterjee D, Shi WT, Forsberg F. Material characterization of the encapsulation of an ultrasound contrast microbubble and its subharmonic response: Strain-softening interfacial elasticity model. J Acoust Soc Am 2010;127:3846–57.
[36] Goel L, Wu H, Zhang B, Kim J, Dayton PA, Xu Z, et al. Nanodroplet-mediated catheter-directed sonothrombolysis of retracted blood clots. Microsyst Nanoeng 2021;7:1–7.
[37] Tan ZQ, Ooi EH, Chiew YS, Foo JJ, Ng EYK, Ooi ET. A computational framework for the multiphysics simulation of microbubble-mediated sonothrombolysis using a forward-viewing intravascular transducer. Ultrasonics 2023;131:106961.
[38] Wang X, Chen W, Zhou M, Zhang Z, Zhang L. Dynamics of double bubbles under the driving of burst ultrasound. Ultrason Sonochemistry 2022;84:105952.
[39] Huang X, Wang QX, Zhang AM, Su J. Dynamic behaviour of a two-microbubble system under ultrasonic wave excitation. Ultrason Sonochemistry 2018;43:166–74.
[40] Wang QX, Manmi K. Three dimensional microbubble dynamics near a wall subject to high intensity ultrasound. Phys Fluids 2014;26:032104.
[41] Schmitt C, Henni AH, Cloutier G. Characterization of blood clot viscoelasticity by dynamic ultrasound elastography and modeling of the rheological behavior. J Biomech 2011;44:622–9.
[42] Johnson S, Duffy S, Gunning G, Gilvarry M, McGarry JP, McHugh PE. Review of mechanical testing and modelling of thrombus material for vascular implant and device design. Ann Biomed Eng 2017;45:2494–508.
[43] Sugerman GP, Kakaletsis S, Thakkar P, Chokshi A, Parekh SH, Rausch MK. A whole blood thrombus mimic: constitutive behavior under simple shear. J Mech Behav Biomed Mater 2021;115:104216.
[44] Li H, Flé G, Bhatt M, Qu Z, Ghazavi S, Yazdani L, et al. Viscoelasticity imaging of biological tissues and single cells using shear wave propagation. Front Phys 2021;9:666192.